NANO LETTERS

Letter

pubs.acs.org/NanoLett

Real-Time Nanoscale Open-Circuit Voltage Dynamics of Perovskite Solar Cells

Joseph L. Garrett,[†,‡] Elizabeth M. Tennyson,[†,§] Miao Hu,[∥] Jinsong Huang,[∥] Jeremy N. Munday,[*,†,⊥] and Marina S. Leite[*,†,§]

[†]Institute for Research in Electronics and Applied Physics, [‡]Department of Physics, and [§]Department of Materials Science and Engineering, University of Maryland, College Park, Maryland 20742, United States

[∥]Department of Mechanical Engineering, University of Nebraska, Lincoln, Nebraska 68588, United States

[⊥]Department of Electrical and Computer Engineering, University of Maryland, College Park, Maryland 20742, United States

Supporting Information

ABSTRACT: Hybrid organic−inorganic perovskites based on methylammonium lead ($MAPbI_3$) are an emerging material with great potential for high-performance and low-cost photovoltaics. However, for perovskites to become a competitive and reliable solar cell technology their instability and spatial variation must be understood and controlled. While the macroscopic characterization of the devices as a function of time is very informative, a nanoscale identification of their real-time local optoelectronic response is still missing. Here, we implement a four-dimensional imaging method through illuminated heterodyne Kelvin probe force microscopy to spatially (<50 nm) and temporally (16 s/scan) resolve the voltage of perovskite solar cells in a low relative humidity environment. Local open-circuit voltage (V_{oc}) images show nanoscale sites with voltage variation >300 mV under 1-sun illumination. Surprisingly, regions of voltage that relax in seconds and after several minutes consistently coexist. Time-dependent changes of the local V_{oc} are likely due to intragrain ion migration and are reversible at low injection level. These results show for the first time the real-time transient behavior of the V_{oc} in perovskite solar cells at the nanoscale. Understanding and controlling the light-induced electrical changes that affect device performance are critical to the further development of stable perovskite-based solar technologies.

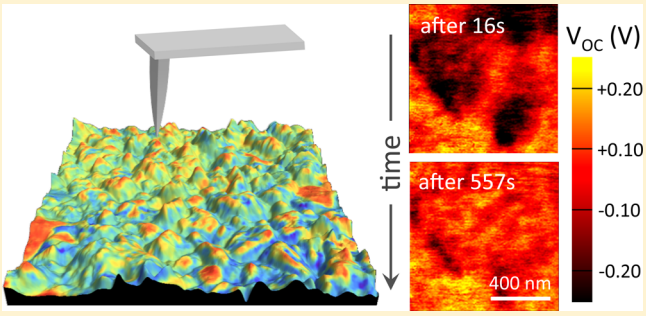

KEYWORDS: *Perovskite, solar cells, photovoltaic, nanoscale imaging, open-circuit voltage*

Recent improvements in power conversion efficiency of perovskite solar cells have brought this class of materials to the same performance level as thin-film CdTe and CIGS photovoltaics, demonstrating its promise as a large-scale technology.[1−4] To date, the world record single-junction perovskite device has a power conversion efficiency of η = 22.1%.[5] Moreover, perovskites are ideal for composing dual-junction designs with a Si or a CIGS bottom subcell.[6,7] The remarkable performance of perovskite solar cells is primarily attributed to their high absorption combined with extremely long carrier diffusion lengths,[8] including one literature report of >175 μm.[9] Despite the rapid progress of the field, there is still a lack of understanding of why and how the material is changing/degrading when exposed to light and humidity.[10,11] Thus, there is a pressing need in the scientific community to elucidate what causes the perovskite active layer to change when the device is operating[12] (exposed to light). Macroscopic electrical measurements, such as light current−voltage (I−V) curves as a function of time, are extremely useful to track the device instabilities;[13,14] however, one cannot infer how much variation exists from grain to grain and within one grain in the perovskite layer, which is needed to determine how the local changes affect the overall device performance.

Microscopy measurements provide a powerful framework for correlating the morphology of the active layers of the solar cells with fundamental physical processes and device performance.[15−18] In particular, scanning microscopy techniques are ideal for investigating heterogeneity at the nanoscale,[19−21] such as the spatial domains on $MAPbI_3$.[21] Recently, micron-scale photoluminescence has been applied to resolve charge carrier recombination and ion migration in perovskite grains.[19,22,23] Through piezo force microscopy, the ferroelectric domains of the perovskites have been observed.[24,25] By time-dependent Kelvin probe measurements, it has been suggested that the hysterisis behavior commonly observed in perovskite devices could be related to trapped charges and ion migration across the light absorbing layer.[26] Kelvin probe force microscopy (KPFM)[27,28] has been used to map the electrostatic potential

Received: January 20, 2017
Revised: February 19, 2017
Published: February 22, 2017

DOI: 10.1021/acs.nanolett.7b00289
Nano Lett. 2017, 17, 2554−2560

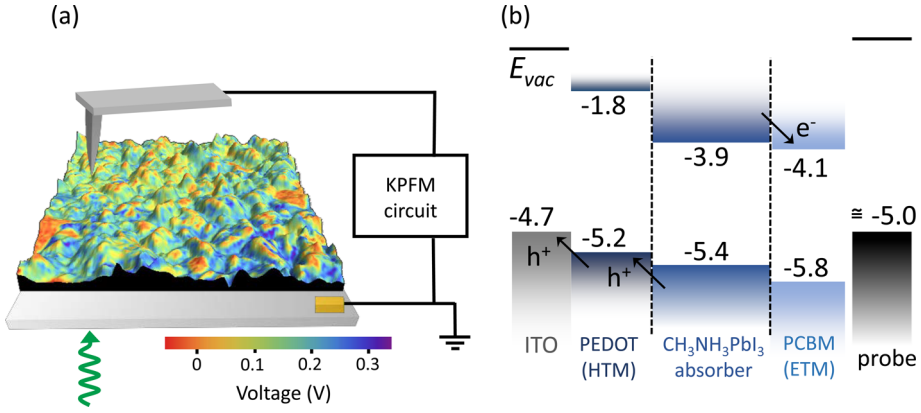

Figure 1. Real-time nanoscale measurements of voltage dynamics in perovskite solar cells. (a) Schematic of hybrid perovskite solar cells measured by illuminated-KPFM, which is out of scale for clarity. The local voltage is overlaid with topography, and the green arrow indicates the illumination direction. (b) Energy diagram of perovskite device and AFM probe illustrating the charge separation mechanism within the hybrid solar cell under illumination. E_{vac} refers to the vacuum energy level, and all energy values are in units of electronvolts. The ITO layer is grounded with respect to the KPFM probe; thus, the subtraction of an illuminated-KPKM scan from a dark-KPKM scan provides a map of the open-circuit voltage of the device. ETM, electron transport material; HTM, hole transport material.

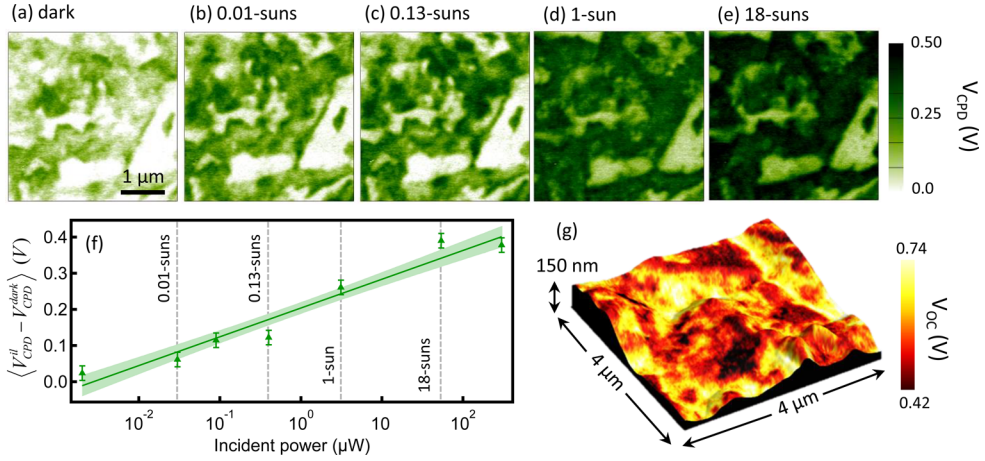

Figure 2. Imaging nanoscale variations in the V_{oc} of perovskite solar cells. (a) Dark-KPFM and (b–e) intensity-dependent illuminated-KPFM scans measured on a perovskite device showing local variations in voltage. (f) Scan-averaged illuminated minus dark voltage ($\langle V_{CPD}^{il} - V_{CPD}^{dark} \rangle$) as a function of incident power (light intensity). The error bars refer to the standard deviation of the averaged values, the green line is the best fit, and the green region represents two deviations from the mean. (g) Absolute V_{oc} map with nanoscale spatial resolution at 1-sun illumination, overlaid with topography.

across multiple layers of active devices,[29,30] to measure work function changes during device poling,[31] and to probe the effect of grain boundaries on $MAPbI_3$.[32] Further, KPFM has been applied to investigate the possible origins of the hysteresis commonly observed in light I–V measurements.[33] Despite these advances, traditional high-resolution variants of atomic force microscopy (AFM) operate too slowly to spatially analyze dynamic events, such as structural changes, light induced chemical reactions, and ion migration.

Here, we image in real-time the dynamics of perovskite solar cells with nanoscale spatial resolution (<50 nm) by mapping local changes in the open-circuit voltage (V_{oc}) through high-speed illuminated-KPFM (16 s/scan), see Figure 1a. For that we implement a novel KPFM method that preserves the spatial sensitivity while increasing the scan speed by >100 times when compared to conventional frequency-modulated-KPFM, where we map nanoscale voltage domains that vary by >300 mV under 1-sun illumination. The voltage within a perovskite grain changes substantially (both spatially and temporally) post light exposure, where regions out of and in equilibrium coexist and are attributed here to intragrain ion migration. We determine the spatial distribution of the local photogenerated voltage, how it varies as a function of time, and we quantify its dynamic behavior as the perovskite solar cell reaches its steady state at over 9 min. A time-dependent residual V_{oc} that lasts for minutes is found, resulting from ion migration, even under dark conditions. Our results demonstrate for the first time the transient electrical behavior of perovskite solar cells with nanoscale spatial resolution.

The solar cells are fabricated by the sequential spin-coating deposition of the perovskite layer ($CH_3NH_3PbI_3$) and the [6,6]-phenyl C_{61}-butyric acid methyl ester (PCBM) layer. The devices are composed of grains ~1 μm in size and with a low density of pinholes with V_{oc} = 1.02 ± 0.02 V (see Figures S1 and S2 for macroscopic device characterization and SEM images). The details concerning sample fabrication are described in the Supporting Information. The band diagram for the device is presented in Figure 1b, where the approximate values of the energy gaps were obtained from refs 3 and 34–38. Here, the PCBM layer functions as the electron transport

DOI: 10.1021/acs.nanolett.7b00289
Nano Lett. 2017, 17, 2554–2560

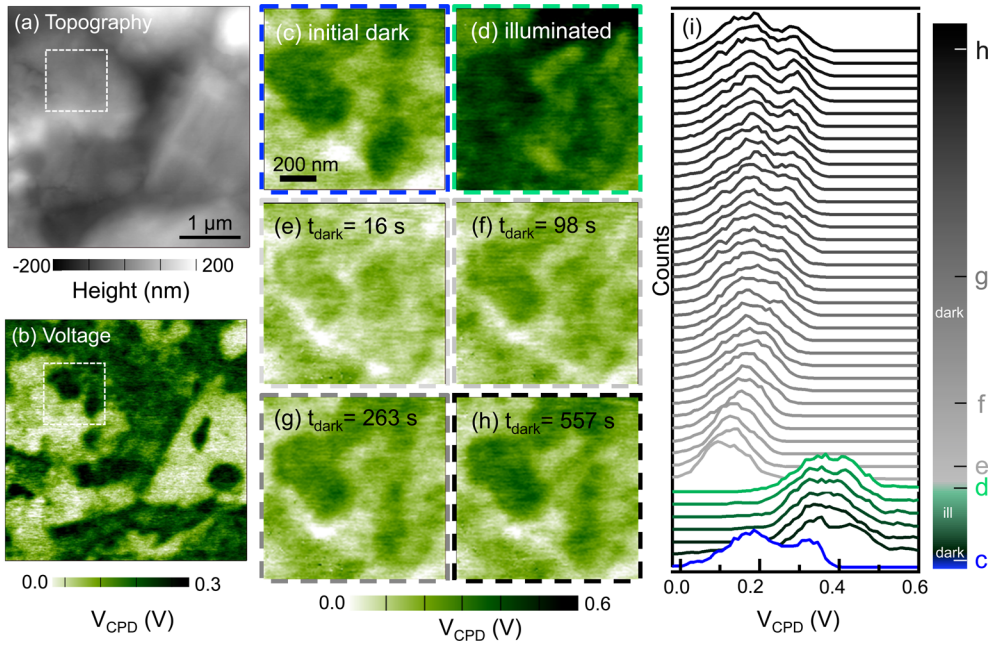

Figure 3. Dynamics of perovskite solar cells at the nanoscale. (a) Topography and (b) dark-KPFM measurements on a representative area of a perovskite photovoltaic device. A sequence of fast-KPFM measurements were acquired on the region highlighted by the white dashed square in (a,b): (c) dark-KPFM, (d) illuminated-KPFM, (e–h) dark-KPFM scans as a function of time. Note that after exposure to light (scan d), it takes the material ~9 min to return to equilibrium (scan h). (i) Histograms of voltage distribution as a function of time for 42 KPFM scans (dark and illuminated) showing reversible dynamics upon a sequence of dark scans. Illumination conditions: 500 nm laser light at 54 μW. Relative humidity <15%.

material (ETM) whereas the PEDOT layer is the hole transport material (HTM), where the holes are preferentially collected through the indium tin oxide (ITO) electrical contact. The perovskite absorbing layer with nominal thickness of 300 nm is sandwiched by the PEDOT and the PCBM (see Figure S1).

We implement two types of KPFM to spatially resolve nanoscale changes of the voltage in the perovskite solar cell. KPFM measures the contact potential difference voltage signal (V_{CPD}), which is proportional to the difference between the work function of the conductive probe and the surface of the sample being scanned. To map the local voltage response in large areas of the device, frequency-modulated KPFM[39−41] can be used (Supporting Information). To increase the scan speed of AFM techniques, common approaches include the use of polymeric cantilevers[42] or to reduce the size of the cantilevers while imaging the sample in an aqueous solution.[43] Although these methods are extremely useful to probe the topography of a variety of materials, they cannot be implemented to accurately measure voltage. Thus, to investigate the perovskites' electrical properties in real-time upon illumination, we realize a variant of heterodyne-KPFM, which enables fast scanning (16 s/scan) while maintaining high spatial resolution.[44] Briefly, the frequency at which the voltage is detected is separated from the frequencies of both the topography feedback loop and the applied voltage[44,45] (see Supporting Information for detailed description of these measurements and Figure S3 for maps of all relevant signals).

In order to better understand the voltage changes that occur under illumination, we perform light intensity dependent in situ measurements of the photogenerated voltage on a large, 16 μm^2, area of the perovskites using KPFM. Figure 2b–e shows a sequence of illuminated-KPFM images from 2 nW to 54 μW (corresponding to low injection level). As the power of the incident light increases, so does the magnitude of the average V_{CPD} (despite the local variations in voltage, as discussed later in this manuscript). Figure 2f shows the expected linear increase of the averaged change in V_{CPD} under illumination, as a function of light intensity.

KPFM has been recently demonstrated as a novel method to map the local V_{oc} of half and fully processed photovoltaic devices with nanoscale spatial resolution, where V_{oc} is the voltage across a solar cell at open-circuit condition. In the illuminated- and dark-KPFM measurements presented here, the voltage on the conductive probe is referenced to the grounded ITO bottom contact. As a result, when the device is illuminated the splitting of the quasi-Fermi level (proportional to the V_{oc} of the solar cell) is directly measured by subtracting an illuminated- from a dark-KPFM scan. Here, we illuminate a well-defined area of the solar cell at normal incidence and thus the local V_{oc} can be expressed as

$$V_{oc}(x, y) = [V_{CPD}^{il}(x, y) - V_{CPD}^{dark}(x, y)] - \beta' \quad (1a)$$

where (x,y) are the spatial coordinates, il and dark refer to illuminated and dark conditions, and

$$\beta' = \frac{nkT}{q}\left[\ln\left(\frac{A_{il}}{A_{cell}} + \frac{J_{dark}}{J_{sc}}\right)\right] \quad (1b)$$

at 1-sun illumination, where n is the ideality factor (obtained from the slope of the curve shown in Figure 2f), k is Boltzmann's constant, T is the temperature, A_{cell} = 1.0 cm^2 and A_{il} = 2.0 × 10^{-3} cm^2 are the total cell and illuminated areas, respectively, and J_{dark} and J_{sc} are the dark current and short-circuit current densities. The coefficient β' (= −0.22 ± 0.03 V) is a calibration factor that depends on the illumination conditions and on the area of the device being probed. Note that when the whole cell is illuminated, β' = 0, as $A_{il} = A_{cell}$ and

DOI: 10.1021/acs.nanolett.7b00289
Nano Lett. 2017, 17, 2554−2560

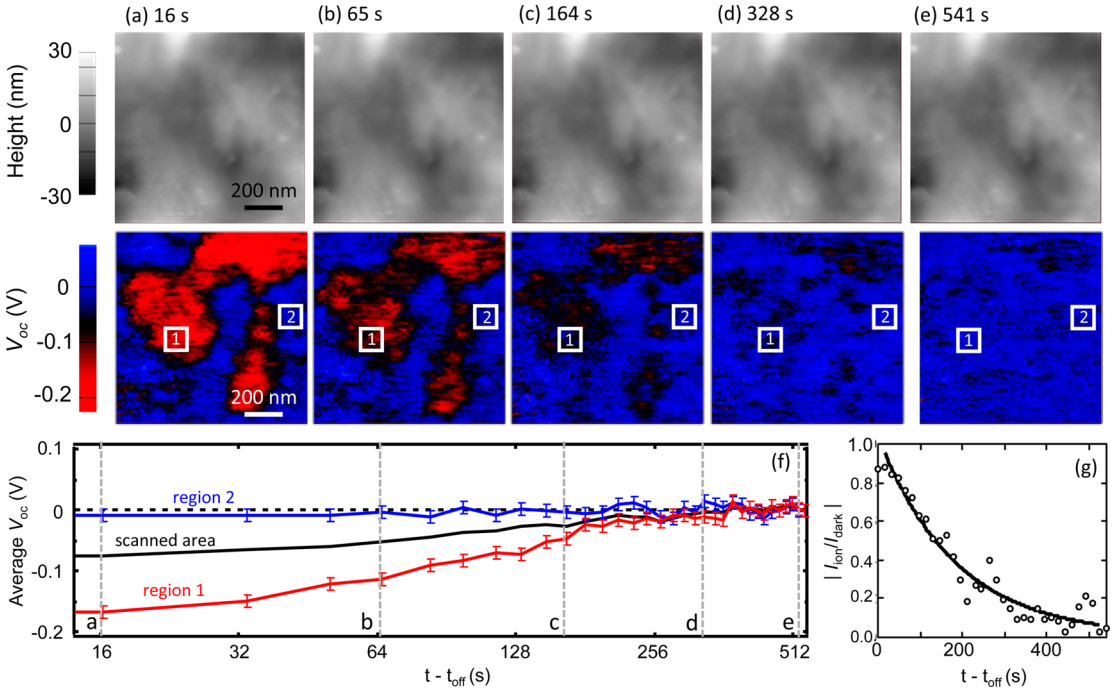

Figure 4. Spatial and temporal variation of the residual photogenerated voltage within perovskite solar cells. Topography and V_{oc} scans acquired after the solar cell is illuminated and brought back to dark conditions after (a) 16, (b) 65, (c) 164, (d) 328, and (e) 541 s. Note that immediately after illumination two distinct regions are observed, one with V_{oc} equal zero (blue) and another with V_{oc} = −0.2 V (red). (f) Averaged V_{oc} as a function of time for the entire scanned area shown in (a−e) (black) and for regions 1 and 2 (highlighted by the white squares). The error bars refer to three standard deviations from the averaged values. The vertical gray dashed lines correspond to the time interval where the scans (a−e) are performed. (g) Ratio of current due to ion migration (I_{ion}) and dark current (I_{dark}) as a function of time. Black line is an exponential fit to the experimental data resulting in a time constant of 185 ± 27 s.

$J_{sc} \gg J_{dark}$. Figure 2g shows a representative V_{oc} map for the perovskite solar cell under 1-sun local illumination, which exhibits spatial variations >300 mV. These remarkable changes in photovoltage demonstrate that the material's electrical characteristics vary locally from grain to grain and within a single grain. The average value of the V_{oc} measured by KPFM is smaller than the initial value obtained by macroscopic light $I-V$ measurements immediately after fabrication (see Figure S1), which primarily results from the V_{oc} decay of the sample at a rate of ∼5% per day (see the inset of Figure S1).

Figure 3a,b shows representative topography and KPFM scans in a 16 μm^2 region of the perovskite device in the dark (at equilibrium). The V_{CPD} varies spatially with a standard deviation of 80 mV (substantially greater than the noise) and is independent of the morphology of the sample. These spatial variations could be due to inhomogeneities either within the perovskite or within the PCBM layer, caused by the spin coating deposition process used to fabricate the sample. During all measurements presented here, the temperature was kept at 28−29 °C and the relative humidity <15% inside the AFM enclosure, see Figure S4 for stability of the environment inside the AFM chamber during dark and illuminated measurements. Figure 3c−h shows the in situ changes in the voltage before, during, and after illumination, obtained by fast-KPFM (16 s/scan), with 54 μW of incident power at wavelength of 500 nm (see Movie S1). According to the KPFM initial dark scan, areas of both high and low surface potential coexist (Figure 3c), with an average V_{CPD} of 0.2 V. Upon illumination, Figure 3d, the surface potential increases substantially, to 0.4 V on average, as a result of the photogenerated voltage. No change in topography is observed during the KPFM scans (see Figure S5), indicating that these perovskite devices are morphologically stable during this time frame under the illumination conditions and the environment used in this experiment. Surprisingly, after turning the light back OFF a transient decay of the voltage is observed, see Figure 3e−h. Over time, the voltage returns toward its initial profile, where it takes ∼9 min for the material to achieve its original surface potential spatial distribution (Figure 3h).

Through the voltage histograms displayed in Figure 3i we quantify this complex transient behavior of the perovskite's voltage. Each pixel in a 128 × 128 pixel map is binned according to its voltage value to produce the histograms. Note how the spatial distribution of the voltage changes with time until the device reaches equilibrium again. In particular, the histograms reveal that the initial dark voltage distribution (blue) is quite broad with a peak around 0.2 V, and under illumination this distribution increases to 0.4 V (green curves). However, after turning the laser OFF, the potential immediately becomes a single, fairly narrow Gaussian (light gray curve). As time progresses, the V_{CPD} broadens again, primarily by extending to higher voltages (dark gray curves). This behavior is also observed after exposing the perovskite to different illumination intensities (ranging from 2.0 nW to 4.2 mW, see Figure S6). These results demonstrate that after exposing the perovskite to light, its voltage changes as a function of time even under dark conditions.

Another striking observation about these perovskite solar cells is that upon removing the illumination the V_{oc} does not immediately return to zero. Instead, a nonzero average voltage persists for several minutes with a sign that is opposite of the V_{oc} under illumination. This behavior is consistent with trap

DOI: 10.1021/acs.nanolett.7b00289
Nano Lett. 2017, 17, 2554−2560

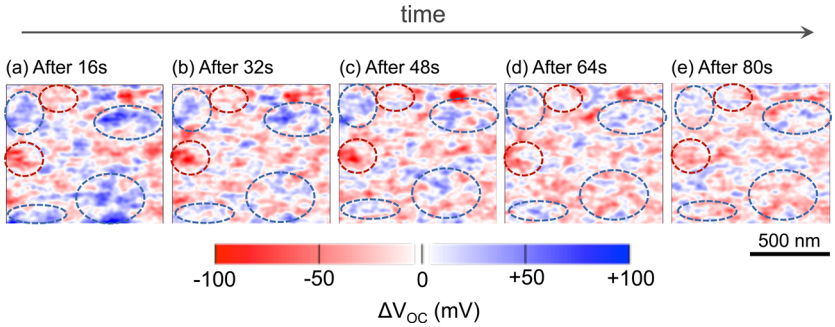

Figure 5. Real-time nanoscale V_{oc} dynamics of perovskite photovoltaics. Sequence of ΔV_{oc} maps as a function of time after (a) 16, (b) 32, (c) 48, (d) 64, and (e) 80 s of illumination. Each scan is subtracted from an illuminated one after 96 s (from Figure 3i). The blue and red dashed areas highlight regions with transient voltage response. The scans size is 1 × 1 μm^2.

filling and subsequent ion migration, which have been observed to take minutes to equilibrate on the macroscale.[46,47] To quantify the time-dependent voltage response within the perovskite solar cell, we analyze the spatial variation of this residual V_{oc} obtained by subtracting the equilibrium dark-KPFM image, Figure 3h, from the postillumination dark-KPFM scans, see, for example, Figures 3e–g. Figure 4 displays the residual V_{oc} images for the perovskite solar cell for a series of snapshots. The dark measurement immediately after turning the laser OFF shows a transient electrical behavior (Figure 4a), most likely resulting from a reversible electronic process within the material. The representative scans shown in Figure 4a–e have two very distinct regions with initial V_{oc} = −0.2 V (red) and V_{oc} = 0 V (blue), revealing a strong bimodal voltage distribution on the electrical response of the device, not resolved by conventional macroscopic electrical measurements or by standard AFM-based methods. As the system approaches equilibrium, the V_{oc} in the initially red region approaches zero, see voltage scans in Figure 4b–e, while the blue regions remain unchanged. Figure 4f shows the averaged V_{oc} as a function of time for the entire scanned area shown in (a–e) (black curve) and the voltage for the regions highlighted by the white squares (red and blue curves). Each point on the graph corresponds to the averaged value (either within the white squares or for the entire scanned region). Here, the variance is calculated by considering each pixel in each box as an individual measurement with 30 mV standard deviation, and it is plotted at three standard deviations. The blue curve is constant under dark conditions (laser OFF), indicating that either some regions of the PCBM layer do not suffer any postillumination driven electrical changes or that these regions return to equilibrium in less than 16 s. Nevertheless, the red curve shows that an out-of-equilibrium state persists for several minutes. These time-dependent measurements reveal that the voltage equilibration has a spatial dependence at the nanoscale that could be responsible for the light-dependent instability observed in perovskites.[48]

Because no net current flows out of the device at open-circuit conditions, an additional current term must balance the diode dark current (I_{dark}) to enable a residual voltage to exist without illumination. We explain this behavior using a simple diode model with an additional time-dependent current term, $I_{ion}(t)$, which could arise as a result of ion migration and/or a change in the density of trap states

$$I(V) = I_L - I_{dark}[e^{qV/nkT} - 1] + I_{ion}(t) \quad (2a)$$

where I_L is the light-generated current of the solar cell. In the dark (I_L = 0), and at open-circuit conditions we have

$$I_{ion}(t) = I_{dark}[e^{qV_{oc}(t)/nkT} - 1] \quad (2b)$$

where $V_{oc}(t)$ is the time-dependent residual open-circuit voltage. Postillumination, $I_{ion}(t)$ opposes the original dark current and tends toward zero on the time scale of minutes. Figure 4g shows the decay of $I_{ion}(t)$ as the device reaches equilibrium, resulting in a time constant of 185 ± 27 s.

As one of the primary limiting factors of perovskite photovoltaics is the material instability when exposed to light, we also measure the time-dependent local changes in V_{oc} under illumination, as presented in Figure 5. Here, we determine ΔV_{oc} by the difference between two illuminated KPFM maps, where each resulting scan corresponds to an instant of time subtracted from the last illuminated one in Figure 3i (as highlighted in light green). The sequence of ΔV_{oc} maps show the local spatial variation in the photogenerated voltage. As previously observed,[46] when the perovskite material is illuminated, the trap states due to vacancies are filled by electrons. As a result, the ions move away from these sites (due to electrostatic repulsion). We track this ion migration process in real-time by spatially resolving changes in the local voltage (ΔV_{oc}) that take place during material illumination. We hypothesize that ions migrate away from the PCBM layer (electron transport layer) due to the built-in electric field. Regions with $\Delta V_{oc} > 0$ and < 0 coexist, strongly indicating that there is an accumulation of ions and vacancies within the illuminated area of the cell, which varies in time. At low injection level, this migration process is reversible and does not lead to material degradation. Yet, it changes the electrical behavior of the device locally, which ultimately affects the overall performance of the solar cells.

We attribute the dynamic behavior of the local electrical response of the perovskite solar cell mapped here to intragrain ion migration:[23,31] charge accumulation takes place when the material is illuminated, and charge migration when the solar cell is no longer in operation (dark conditions). This photoinduced ion migration is primarily driven by the movement of ions to depleted regions, as observed in prior photoluminescence experiments.[23] We demonstrate that this phenomenon is fully reversible at low illumination injection level (Figure 2) and does not result in permanent material degradation. Further, the spatial variations in the local electrical response are not accompanied by any changes in morphology (see Figure S5 for sequence of topography maps during material illumination) but the nanoscale time-dependent variations are most likely responsible for macroscopic instabilities observed in these

DOI: 10.1021/acs.nanolett.7b00289
Nano Lett. 2017, 17, 2554–2560

perovskite solar cells. The diffusion of ions under dark conditions leads to a time-dependent local residual $V_{oc}(t)$, mapped here for the first time. Our results indicate that free carriers are probably responsible for the observed transient voltage. Once the material is under dark conditions again, some ions continuously move until the perovskite layer achieves an equilibrium state, which takes place in several minutes for the material probed in this work (as shown in Figure 3).

The real-time functional imaging method reported here can be combined with other scanning probe microscopies and big data analysis[49] to probe additional relevant phenomena that currently describes the unique illumination-dependent behavior of perovskites, such as structural transformation,[50] ferroelectric domains,[24,51] poling[46] and piezoelectric behavior.[24] For instance, to map structural and chemical composition changes fast-KPFM could be combined with tip-enhanced Raman spectroscopy. Likewise, to investigate the possible effects of long-lived traps[52] on the device's local electrical response our novel imaging method could be combined with pump−probe EFM/KPFM techniques,[53,54] which measure voltage at microsecond time scales. Further, spectrally dependent fast-KPFM could help elucidate the mechanism responsible for light-induced self-poling in perovskites.

In summary, we imaged and quantified the real-time voltage dynamics of perovskite solar cells at the nanoscale (<50 nm) under illumination and postillumination conditions by fast KPFM (16 s/scan) in a low relative humidity environment. One-sun local V_{oc} maps of the perovskites revealed absolute variations >300 mV between and within grains. Under illumination, the photogenerated voltage of the perovskite varied spatially within one grain. After illumination, it took the material ∼9 min to reach its equilibrium state. This transient electrical behavior, most likely resulting from reversible ion migration within the perovskite layer, cannot be revealed by conventional macroscopic electrical measurements. The real-time nanoscale imaging experiments presented here demonstrate that the V_{oc} (electrical response) of perovskite photovoltaics varies locally and that light-induced reversible ion migration could be responsible for the time-dependent transient behavior of most perovskite photovoltaics. Substantial effort lies ahead to acquire a full picture of the mechanism(s) responsible for the light-induced physical and chemical processes frequently observed in this class of materials and their effects on the maximum attainable open-circuit voltage. Nevertheless, our nanoscale time-dependent measurement represents a new imaging method to diagnose the local electrical response of perovskites, ranging from lead-free $CsBrI_xBr_{3-x}$ alternatives to $FAPbX_3$ and $MAPb[I_{(1-x)}Br_x]_3$ for optimized dual-junction solar cells and for light-emitting applications. Thus, mapping the spatial and time dynamics of perovskite materials will likely impact the design of next-generation stable perovskite solar cells with reliable voltage response.

■ ASSOCIATED CONTENT

Supporting Information

The Supporting Information is available free of charge on the ACS Publications website at DOI: 10.1021/acs.nanolett.7b00289.

Macroscale characterization, humidity control, additional topography scans, and voltage histograms (PDF)

Changes in the voltage before, during, and after illumination obtained by fast-KPFM (MPG)

■ AUTHOR INFORMATION

Corresponding Authors

*E-mail: mleite@umd.edu.
*E-mail: jnmunday@umd.edu.

ORCID

Jinsong Huang: 0000-0002-0509-8778
Jeremy N. Munday: 0000-0002-0881-9876
Marina S. Leite: 0000-0003-4888-8195

Author Contributions

M.S.L. conceived the research idea. J.L.G., E.M.T., J.N.M., and M.S.L. designed the experiments and analyzed the data. J.L.G. and E.M.T. performed the KPFM measurements. M.U. and J.H. fabricated the perovskite solar cells and performed the macroscopic characterization. M.S.L., J.N.M., J.L.G., and E.M.T. wrote the article and all authors commented on and edited the manuscript.

Notes

The authors declare no competing financial interest.

■ ACKNOWLEDGMENTS

The authors thank O. Rabin, A. Lawson, and N. Ballew for technical assistance. J.L.G. and J.N.M. acknowledge funding from the UMD Department of Physics through The Thomas Mason Interdisciplinary Physics Fund, E.M.T. thanks the 2015 Summer Graduate Fellowship Award and the 2016/2017 Dean's Fellowship, and M.S.L. thanks NSF-ECCS and the 2015 RASA/UMD Award. The authors also acknowledge the financial support from the National Science Foundation (ECCS-1610833, DMR-1505535, and DMR-1420645).

■ REFERENCES

(1) Green, M. A.; Ho-Baillie, A.; Snaith, H. J. *Nat. Photonics* **2014**, *8*, 506−514.
(2) Brenner, T. M.; Egger, D. A.; Kronik, L.; Hodes, G.; Cahen, D. *Nat. Rev. Mater.* **2016**, *1*, 15007.
(3) Gao, P.; Gratzel, M.; Nazeeruddin, M. K. *Energy Environ. Sci.* **2014**, *7*, 2448−2463.
(4) Sessolo, M.; Bolink, H. J. *Science* **2015**, *350*, 917−917.
(5) Green, M. A.; Emery, K.; Hishikawa, Y.; Warta, W.; Dunlop, E. D.; Levi, D. H.; Ho-Baillie, A. W. Y. *Prog. Photovoltaics* **2017**, *25*, 3−13.
(6) Mailoa, J. P.; Bailie, C. D.; Johlin, E. C.; Hoke, E. T.; Akey, A. J.; Nguyen, W. H.; McGehee, M. D.; Buonassisi, T. *Appl. Phys. Lett.* **2015**, *106*, 121105.
(7) Bailie, C. D.; Christoforo, M. G.; Mailoa, J. P.; Bowring, A. R.; Unger, E. L.; Nguyen, W. H.; Burschka, J.; Pellet, N.; Lee, J. Z.; Grätzel, M.; Noufi, R.; Buonassisi, T.; Salleo, A.; McGehee, M. D. *Energy Environ. Sci.* **2015**, *8*, 956−963.
(8) Shi, D.; Adinolfi, V.; Comin, R.; Yuan, M.; Alarousu, E.; Buin, A.; Chen, Y.; Hoogland, S.; Rothenberger, A.; Katsiev, K.; Losovyj, Y.; Zhang, X.; Dowben, P. A.; Mohammed, O. F.; Sargent, E. H.; Bakr, O. M. *Science* **2015**, *347*, 519−522.
(9) Dong, Q.; Fang, Y.; Shao, Y.; Mulligan, P.; Qiu, J.; Cao, L.; Huang, J. *Science* **2015**, *347*, 967−970.
(10) Berry, J.; Buonassisi, T.; Egger, D. A.; Hodes, G.; Kronik, L.; Loo, Y.-L.; Lubomirsky, I.; Marder, S. R.; Mastai, Y.; Miller, J. S.; Mitzi, D. B.; Paz, Y.; Rappe, A. M.; Riess, I.; Rybtchinski, B.; Stafsudd, O.; Stevanovic, V.; Toney, M. F.; Zitoun, D.; Kahn, A.; Ginley, D.; Cahen, D. *Adv. Mater.* **2015**, *27*, 5102−5112.
(11) Niu, G.; Guo, X.; Wang, L. *J. Mater. Chem. A* **2015**, *3*, 8970−8980.

DOI: 10.1021/acs.nanolett.7b00289
Nano Lett. 2017, 17, 2554−2560

(12) You, J. B.; Meng, L.; Song, T. B.; Guo, T. F.; Yang, Y.; Chang, W. H.; Hong, Z. R.; Chen, H. J.; Zhou, H. P.; Chen, Q.; Liu, Y. S.; De Marco, N.; Yang, Y. *Nat. Nanotechnol.* **2015**, *11*, 75−81.
(13) Snaith, H. J.; Abate, A.; Ball, J. M.; Eperon, G. E.; Leijtens, T.; Noel, N. K.; Stranks, S. D.; Wang, J. T.-W.; Wojciechowski, K.; Zhang, W. *J. Phys. Chem. Lett.* **2014**, *5*, 1511−1515.
(14) Qiu, W.; Paetzold, U. W.; Gehlhaar, R.; Smirnov, V.; Boyen, H.-G.; Tait, J. G.; Conings, B.; Zhang, W.; Nielsen, C. B.; McCulloch, I.; Froyen, L.; Heremans, P.; Cheyns, D. *J. Mater. Chem. A* **2015**, *3*, 22824.
(15) Tennyson, E. M.; Garrett, J. L.; Frantz, J. A.; Myers, J. D.; Bekele, R. Y.; Sanghera, J. S.; Munday, J. N.; Leite, M. S. *Adv. Energy Mater.* **2015**, *5*, 1501142.
(16) Leite, M. S.; Abashin, M.; Lezec, H. J.; Gianfrancesco, A.; Talin, A. A.; Zhitenev, N. B. *ACS Nano* **2014**, *8*, 11883−11890.
(17) Leite, M. S.; Abashin, M.; Lezec, H. J.; Gianfrancesco, A.; Talin, A. A.; Zhitenev, N. B. J. *IEEE J. Photovoltaics* **2014**, *4*, 311−316.
(18) Tennyson, E. M.; Frantz, J. A.; Howard, J. M.; Gunnarsson, W. B.; Myers, J. D.; Bekele, R. Y.; Sanghera, J. S.; Na, S.-M.; Leite, M. S. *ACS Energy Letters* **2016**, *1*, 899−905.
(19) Vrućinić, M.; Matthiesen, C.; Sadhanala, A.; Divitini, G.; Cacovich, S.; Dutton, S. E.; Ducati, C.; Atatüre, M.; Snaith, H.; Friend, R. H.; Sirringhaus, H.; Deschler, F. *Adv. Sci.* **2015**, *2*, 1500136.
(20) Leblebici, S. Y.; Leppert, L.; Li, Y.; Reyes-Lillo, S. E.; Wickenburg, S.; Wong, E.; Lee, J.; Melli, M.; Ziegler, D.; Angell, D. K.; Ogletree, D. F.; Ashby; Paul, D.; Toma, F. M.; Neaton, J. B.; Sharp, I. D.; Weber-Bargioni, A. *Nat. Energy* **2016**, *1*, 16093.
(21) Kutes, Y.; Zhou, Y.; Bosse, J. L.; Steffes, J.; Padture, N. P.; Huey, B. D. *Nano Lett.* **2016**, *16*, 3434−3441.
(22) de Quilettes, D. W.; Vorpahl, S. M.; Stranks, S. D.; Nagaoka, H.; Eperon, G. E.; Ziffer, M. E.; Snaith, H. J.; Ginger, D. S. *Science* **2015**, *348*, 683−686.
(23) deQuilettes, D. W.; Zhang, W.; Burlakov, V. M.; Graham, D. J.; Leijtens, T.; Osherov, A.; Bulovic, V.; Snaith, H. J.; Ginger, D. S.; Stranks, S. D. *Nat. Commun.* **2016**, *7*, 11683.
(24) Kutes, Y.; Ye, L.; Zhou, Y.; Pang, S.; Huey, B. D.; Padture, N. P. *J. Phys. Chem. Lett.* **2014**, *5*, 3335−3339.
(25) Beilsten-Edmands, J.; Eperon, G. E.; Johnson, R. D.; Snaith, H. J.; Radaelli, P. G. *Appl. Phys. Lett.* **2015**, *106*, 173502.
(26) Bergmann, V. W.; Guo, Y.; Tanaka, H.; Hermes, I. M.; Li, D.; Klasen, A.; Bretschneider, S. A.; Nakamura, E.; Berger, R.; Weber, S. A. L. *ACS Appl. Mater. Interfaces* **2016**, *8*, 19402−19409.
(27) Zerweck, U.; Loppacher, C.; Otto, T.; Grafström, S.; Eng, L. M. *Phys. Rev. B: Condens. Matter Mater. Phys.* **2005**, *71*, 125424.
(28) Weaver, J. M. R.; Abraham, D. W. *J. Vac. Sci. Technol., B: Microelectron. Process. Phenom.* **1991**, *9*, 1559−1561.
(29) Bergmann, V. W.; Weber, S. A. L.; Javier Ramos, F.; Nazeeruddin, M. K.; Grätzel, M.; Li, D.; Domanski, A. L.; Lieberwirth, I.; Ahmad, S.; Berger, R. *Nat. Commun.* **2014**, *5*, 5001.
(30) Jiang, C.-S.; Yang, M.; Zhou, Y.; To, B.; Nanayakkara, S. U.; Luther, J. M.; Zhou, W.; Berry, J. J.; Lagemaat, J. v. d.; Padture, N. P.; Zhu, K.; Al-Jassim, M. M. *Nat. Commun.* **2015**, *6*, 8397.
(31) Xiao, Z.; Yuan, Y.; Shao, Y.; Wang, Q.; Dong, Q.; Bi, C.; Sharma, P.; Gruverman, A.; Huang, J. *Nat. Mater.* **2014**, *14*, 193−198.
(32) Yun, J. S.; Anita, H.-B.; Shujuan, H.; H, W. S.; Yooun, H.; Jan, S.; Fuzhi, H.; Yi-Bing, C.; A, G. M. *J. Phys. Chem. Lett.* **2015**, *6*, 875−880.
(33) Kim, Y. C.; Jeon, N. J.; Noh, J. H.; Yang, W. S.; Seo, J.; Yun, J. S.; Ho-Baillie, A.; Huang, S.; Green, M. A.; Seidel, J.; Ahn, T. K.; Seok, S. I. *Adv. Energy Mater.* **2016**, *6*, 1502104.
(34) Kim, H.-B.; Choi, H.; Jeong, J.; Kim, S.; Walker, B.; Song, S.; Kim, J. Y. *Nanoscale* **2014**, *6*, 6679−6683.
(35) Wang, S.; Sakurai, T.; Kuroda, R.; Akimoto, K. *Jpn. J. Appl. Phys.* **2012**, *51*, 10NE32.
(36) Itoh, E.; Shirotori, T. *Jpn. J. Appl. Phys.* **2012**, *51*, 02BK14.
(37) Jeng, J.-Y.; Chiang, Y.-F.; Lee, M.-H.; Peng, S.-R.; Guo, T.-F.; Chen, P.; Wen, T.-C. *Adv. Mater.* **2013**, *25*, 3727−3732.
(38) Hu, M.; Bi, C.; Yuan, Y.; Xiao, Z.; Dong, Q.; Shao, Y.; Huang, J. *Small* **2015**, *11*, 2164−2169.
(39) Jesse, S.; Balke, N.; Eliseev, E.; Tselev, A.; Dudney, N. J.; Morozovska, A. N.; Kalinin, S. V. *ACS Nano* **2011**, *5*, 9682−9695.
(40) Kumar, A.; Arruda, T. M.; Tselev, A.; Ivanov, I. N.; Lawton, J. S.; Zawodzinski, T. A.; Butyaev, O.; Zayats, S.; Jesse, S.; Kalinin, S. V. *Sci. Rep.* **2013**, *3*, 1621.
(41) Balke, N.; Jesse, S.; Morozovska, A. N.; Eliseev, E.; Chung, D. W.; Kim, Y.; Adamczyk, L.; Garcia, R. E.; Dudney, N.; Kalinin, S. V. *Nat. Nanotechnol.* **2010**, *5*, 749−754.
(42) Adams, J. D.; Erickson, B. W.; Grossenbacher, J.; Brugger, J.; Nievergelt, A.; Fantner, G. E. *Nat. Nanotechnol.* **2015**, *11*, 147−151.
(43) Ando, T.; Kodera, N.; Takai, E.; Maruyama, D.; Saito, K.; Toda, A. *Proc. Natl. Acad. Sci. U. S. A.* **2001**, *98*, 12468−12472.
(44) Garrett, J. L.; Munday, J. N. *Nanotechnology* **2016**, *27*, 245705.
(45) Sugawara, Y.; Kou, L.; Ma, Z.; Kamijo, T.; Naitoh, Y.; Jun, L. Y. *Appl. Phys. Lett.* **2012**, *100*, 223104.
(46) Deng, Y.; Xiao, Z.; Huang, J. *Adv. Energy Mater.* **2015**, *5*, 1−6.
(47) Tress, W.; Marinova, N.; Moehl, T.; Zakeeruddin, S. M.; Nazeeruddin, M. K.; Gratzel, M. *Energy Environ. Sci.* **2015**, *8*, 995−1004.
(48) Yang, J.; Siempelkamp, B. D.; Liu, D.; Kelly, T. L. *ACS Nano* **2015**, *9*, 1955−1963.
(49) Strelcov, E.; Belianinov, A.; Hsieh, Y.-H.; Jesse, S.; Baddorf, A. P.; Chu, Y.-H.; Kalinin, S. V. *ACS Nano* **2014**, *8*, 6449−6457.
(50) Gottesman, R.; Haltzi, E.; Gouda, L.; Tirosh, S.; Bouhadana, Y.; Zaban, A.; Mosconi, E.; De Angelis, F. *J. Phys. Chem. Lett.* **2014**, *5*, 2662−2669.
(51) Frost, J. M.; Butler, K. T.; Brivio, F.; Hendon, C. H.; van Schilfgaarde, M.; Walsh, A. *Nano Lett.* **2014**, *14*, 2584−2590.
(52) Leijtens, T.; Eperon, G. E.; Barker, A. J.; Grancini, G.; Zhang, W.; Ball, J. M.; Kandada, A. R. S.; Snaith, H. J.; Petrozza, A. *Energy Environ. Sci.* **2016**, *9*, 3472−3481.
(53) Karatay, D. U.; Harrison, J. S.; Glaz, M. S.; Giridharagopal, R.; Ginger, D. S. *Rev. Sci. Instrum.* **2016**, *87*, 053702.
(54) Murawski, J.; Graupner, T.; Milde, P.; Raupach, R.; Zerweck-Trogisch, U.; Eng, L. M. *J. Appl. Phys.* **2015**, *118*, 154302.

DOI: 10.1021/acs.nanolett.7b00289
Nano Lett. 2017, 17, 2554−2560